

HoFe - Garnet soft XMCD measurements below and above the compensation temperature

E. Goering, S. Gold and G. Schütz

Lehrstuhl für Experimentalphysik IV, Universität Würzburg, Germany; goering@physik.uni-wuerzburg.de

We have investigated the magnetism of Holmium-Iron-Garnet ($\text{Ho}_3\text{Fe}_5\text{O}_{12}$) at the Ho $M_{4,5}$ - the Fe $L_{2,3}$ - and the O K - edges. As expected switching of the sub-lattice magnetization is observed at the compensation temperature. We will give detailed analysis of the Ho and Fe XMCD signals, using sum rules. Fe dichroism is analyzed in terms of 3d ground state moments and compared to Gadolinium-Iron-Garnet ($\text{Gd}_3\text{Fe}_5\text{O}_{12}$). Contributions of octahedral and tetrahedral Fe sites could be separated and analyzed quantitatively. At the oxygen K edge two different structures are observable. Those structures show different temperature dependencies. Therefore we address these features separately to Fe and Rare Earth contributions.

Keywords: rare earth; transition metals; oxides; X-ray magnetic circular dichroism; sum rules; ferrimagnetism; iron garnets

1. Introduction

Rare earth iron garnets (ReIG or $\text{Re}_3\text{Fe}_5\text{O}_{12}$; $\text{Re} = \text{Ce}, \text{Pr}, \text{Nd}, \text{Pm} \dots$), are the most common textbook standard example for complex ferrimagnetism (Hellwege 1988; Kittel 1976). The structure is complicated and 8 formula units are in a single cubic cell (160 ions) (Geller 1963; Geller 1965). XMCD studies on ReIG have been performed previously in the hard (Fischer 1992; Kawamura 1997; Knulle 1995; Maruyama 1995) and in the soft X-ray range (Rudolf 1991; Rudolf 1992; Sette 1990). Also, the first angular dependent XMCD result was performed at the M_5 edge of TbIG (Van Der Laan 1986). Using X-ray Magnetic Circular Dichroism (XMCD) the ferrimagnetic sub-lattice magnetization could be studied quantitatively using sum rules (Altarelli 1993; Carra 1993; Dartyge 1998; Thole 1992; van der Laan 1998a).

Three different sub-lattices are magnetically interacting and coupled with superexchange by oxygen. In a formula unit 5 Fe^{3+} ions are present, two Fe^{3+} are positioned at octahedral sites (A) and three Fe^{3+} at tetrahedral sites (D), while the Re^{3+} ions are located at pseudo dodecahedral places (C) (Pauthenet 1958). The Fe^{3+} sub-lattices are strongly interacting and they order antiferromagnetic at high temperatures ($T_c = 564 \text{ K}$ for GdIG , 567 K for HoIG). The Curie temperature is approximately independent from the Re element. Therefore YIG can be used as a Fe^{3+} reference, because Y is non magnetic. Each Fe^{3+} ion has a $3d^5$ electron configuration with a Hund's rule ground state of $^6S_{5/2}$ resulting in a magnetic spin moment of $4.4\mu_B$ (Geller 1965). Therefore the resulting total Fe ground state magnetization per formula unit is $4.4\mu_B$ or $0.88\mu_B$ for a single Fe^{3+} ion. The Re^{3+} ions are weakly antiferromagnetic coupled to the total Fe magnetization and the Re magnetization increases slowly below T_c . At room temperature the Fe^{3+} ions are dominating the total magnetization. In an external magnetic field B, the average Fe^{3+} moment is parallel aligned and the Re^{3+} antiparallel. With decreasing temperature, the Re sub-lattice magnetization is increasing and, due to the antiferromagnetic coupling to the Fe, the total magnetization is decreasing. At the so called compensation temperature T_{co} , the total magnetization has

vanished. Below T_{co} ($T_{co} = 290 \text{ K}$ for Gd; 136 K for Ho) the Re ions dominate the magnetization and are parallel to an external magnetic field while the resulting Fe moment is now antiparallel (Neel 1964; Pauthenet 1958). This flipping of the sub-lattice magnetizations could be directly observed in XMCD measurements. In the past, this has been done qualitatively for GdIG (Rudolf 1991; Rudolf 1992; Sette 1990). In our work we have investigated HoIG with XMCD quantitatively. We will discuss the magnetic properties of Fe^{3+} and Re^{3+} in terms of so called Sum Rules (Carra 1993; Thole 1992; Thole 1993). Oxygen K edge XMCD spectra are influenced by the hybridization to the magnetic neighboring ions and Fe^{3+} and Ho^{3+} contributions could be separated by different temperature dependencies.

2. Experimental

Presented X-ray Absorption Spectra (XAS) were recorded at the bending magnet beamline SX 700 III at BESSY I. The monochromator energy resolution was set to $E/\Delta E \approx 1200$ and the degree of circular polarization 0.69 ± 0.05 . All spectra were measured by the total drain current. Two Keithley 6517a were used for measuring simultaneously the sample drain current and the I_0 current from an Au coated Cu grid for normalization. The I_0 grid was positioned in a μ -metal cylinder, to prevent influences of the magnetic field. A split coil superconducting magnet system was used, with a center bore of 5 cm and a maximal field of 30 kOe. The used magnetic field was $\pm 5 \text{ kOe}$.

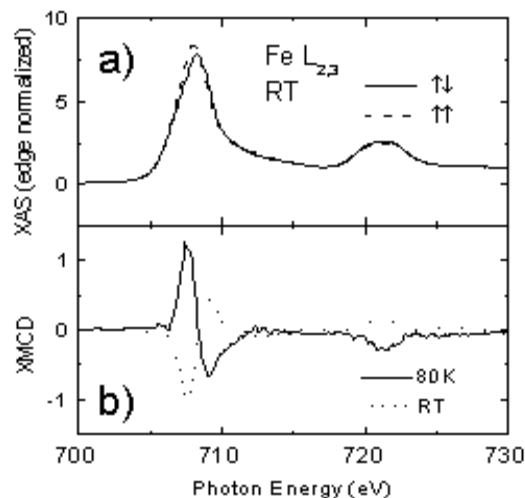


Figure 1: a) Fe $L_{2,3}$ edge normalized absorption spectra at room temperature for antiparallel (line) and parallel (dashed) magnetic fields. b) Corresponding XMCD signal at room temperature (dotted) and 80K (line).

To prevent small XMCD offsets signals, we measured at 80K with an asymmetric magnetic field variation, which does not influence the sample magnetization (Goering 2000). We used an asymmetry field of about 0.2 kOe. All data were recorded by flipping the magnetic field at each data point, to get a derivative free XMCD signal. Samples were measured at 80K and at room temperature (RT). At low temperatures charging of the insulating garnet sample could be prevented by the use of a very thin layer of HoIG powder deposited on colloidal graphite (Aqua Dac), which was used for electrical contact. Charging could further be reduced by dimmed synchrotron light intensities. We had absolute values of sample currents of 3-18 pA for Fe $L_{2,3}$ -, 4-11 pA for O K- and 0.7-3 pA for

Ho $M_{4,5}$ - edges. All shown HoIG XAS and XMCD spectra were background subtracted and edge normalized. For parallel and antiparallel field alignment we use exactly the same background and the same normalization factor, therefore the shape of the dichroism spectrum is not affected.

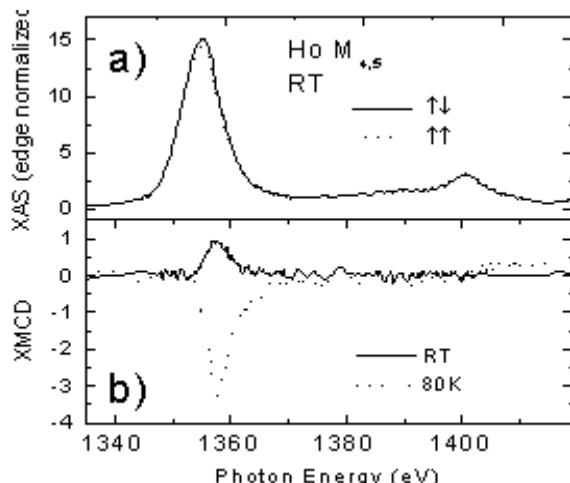


Figure 2: a) Ho $M_{4,5}$ edge normalized absorption spectra at room temperature for antiparallel (line) and parallel (dotted) magnetic fields. b) Corresponding XMCD signal at room temperature (line) and 80K (dotted).

Fig. 1a shows Fe $L_{2,3}$ edge XAS at RT and Fig. 1b XMCD spectra for RT and 80K. The flip of the magnetization above and below T_{CO} and changes in Fe^{3+} sub-lattice magnetization are directly observable. The shape of the XMCD signal is quite different compared to bulk Fe metal (Chen 1995).

In Fig. 2a we show Ho $M_{4,5}$ edge XAS at RT and XMCD spectra for RT and 80K (Fig. 2b). As seen for Fe^{3+} , the flip of the magnetization is also present, but the changes in Ho^{3+} sub-lattice magnetization are much stronger compared to Fe^{3+} . If Ho M_5 XMCD is positive, the Fe L_3 is negative and vice versa, which directly reflects the antiparallel coupling of Fe to Ho.

Fig. 3 shows O K edge XAS (Fig. 3 a) and XMCD (Fig. 3 b) spectra at RT and 80K. No single spectra for $\uparrow\downarrow$ and $\uparrow\uparrow$ magnetic field alignment are shown, because the XMCD signal is in the range of the line thickness. Spectral changes are observable in XAS and XMCD spectra. In the XMCD spectrum, the lowest energy feature at 530 eV changes sign and intensity comparable to the Fe $L_{2,3}$ edge structures in Fig. 1b. Between 535 eV and 540 eV a new magnetic feature is appearing with opposite sign, compared to the first feature at 530 eV.

3. Discussion

As mentioned before, in Fig. 1 - 3 the ferrimagnetic behavior of HoIG is clearly observable (Rudolf 1992). Now we want to discuss all features quantitatively. A sum rule analysis (Carra 1993; Thole 1993) of Fe^{3+} $L_{2,3}$ edge spectra yields to projected orbital and spin moments of Fe 3d electrons. For the nonresonant background we used two step functions (Chen 1995) at the resonance maxima in the XAS signal, with a 2/3 step located at 708.2 eV and 1/3 step at 720.8 eV. We used $n_h = 5$ for the number of holes in the 3d - shell and extract spin moments of $S_z = +0.23 \mu_B$ ($-0.34 \mu_B$) and orbital moments $L_z = +0.03 \mu_B$ ($+0.07 \mu_B$) for RT (80 K) respectively. The ratio between 80 K and RT - S_z values is $-0.34/0.23 = -1.48$. Magnetization data of YIG provides the Fe^{3+} sub-lattice

magnetization and yields to a Fe moment ratio for HoIG of about $4.7\mu_B/3.56\mu_B = 1.34$ (Neel 1964), which is in good agreement to XMCD. The L_z values are very small and - in these measurements - comparable to the noise and error levels.

To extract ground state values for Fe^{3+} we correct for the temperature dependence of the magnetization and for the degree of circular polarization. We use the room temperature values, because these spectra have less noise level compared to 80 K. Therefore we have $0.23\mu_B \cdot 4.7\mu_B/3.56\mu_B / 0.69 = 0.44\mu_B = S_z(0K)$ and $(0.23+0.03)\mu_B \cdot 4.7\mu_B/3.56\mu_B / 0.69 = 0.50\mu_B$ for the total magnetic moment. Fe^{3+} ($3d^5$ configuration) is presumed to be a spin only magnet with about $5 \mu_B/Fe$ Ion and hence an effective $1.0 \mu_B/Fe$ is present in the ferrimagnetic ground state arrangement (Geller 1965). The observed XMCD value is smaller by a factor of 2. To check our result we digitized reference data from Rudolf et al. (Rudolf 1992) for GdIG. Correcting for temperature dependence and circular polarization we get $S_z(GdIG) = 0.59 \mu_B$ and $L_z(GdIG) = 0.22\mu_B$. The L_z value is much greater, compared with our data and inconsistent with the observed spin only ground state magnetization of $4.97\mu_B$ for YIG (Neel 1964) μ_B for LuIG (Geller 1965). For pure metals sum rules seem to be applicable (Chen 1995). We believe that this reduction in projected moments is due to Fe^{3+} hybridization with neighboring O^{2-} ions.

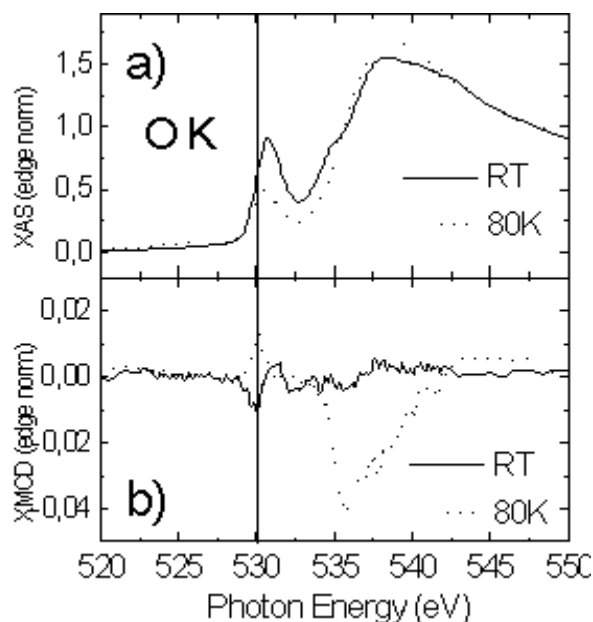


Figure 3: O K edge normalized spectra for room temperature (line) and 80 K (dotted). a) XAS b) XMCD

We performed the same analysis for the Ho $M_{4,5}$ edges. The XMCD measured 4f magnetic moment ratio gives $S_z/L_z = 1$. Taking into account the antiparallel alignment of the Ho 4f spin to the Fe magnetization, we get $S_z/L_z = 4 \mu_B/4.5\mu_B = 0.89$ (Hellwege 1988) for a Hund's rule ground state of a $4f^{10}$ configuration, which is in quite good agreement to the XMCD value of 1. From magnetization we expect a temperature ratio $|\mu^{Ho}(80K)/\mu^{Ho}(RT)| = 3.3$ (Neel 1964). From $M_{4,5}$ - XMCD we get the ratio of $1.02\mu_B/0.28 \mu_B = 3.64$. Calculating the ground state moment for Ho^{3+} with $M^{Ho}(0K)/M^{Ho}(80K) = 17.3\mu_B/7.0\mu_B$ (Neel 1964) we obtain $1.02\mu_B \cdot 17.3\mu_B/7.0\mu_B / 0.69 = 3.7\mu_B$ for Ho 4f. The magnetization gives $17.3\mu_B/3 = 5.8\mu_B$ (Neel 1964). This is a factor of 1.56 compared to our XMCD data. For digitized GdIG data, we get 4f ground state moments of $S_z = 5.6\mu_B$ and $L_z = 1.1\mu_B$. This large L_z value for a Hund's rule spin only system is quite unexpected. The Gd sub lattice magnetization at 0K is $20.0\mu_B$ and $20.0\mu_B/3 = 6.67\mu_B$ per Gd^{3+}

ion (Neel 1964). This is in very good agreement to the XMCD value.

We focus now on the observed temperature dependence of our O K edge spectra (Fig. 3b). The behavior is unusual, because of the arising new feature at 536 eV for low temperatures. We identify near edge spectral features to Fe^{3+} related magnetic interactions, which are consistent to the temperature behavior and to the sign of the XMCD signal compared to Mn induced magnetism in OK edge spectra of $\text{La}_{0.7}\text{Ca}_{0.3}\text{MnO}_3$ (Pellegrin 2000). The new feature at 536 eV has a negative sign at low temperatures and increases dramatically to 80K. We believe that this is related to the Ho^{3+} lattice magnetization. The 4f states are strongly localized and do not overlap significantly with oxygen p electrons. Ho 5d band electrons will hybridize with the O p band and are magnetically polarized by the exchange coupled magnetic 4f electrons. Due to the large number of 160 atoms per unit cell only non-conventional recursive band structure calculations are available for YIG (Dunaevskii 1989)(Dunaevskii 1989) Those 5d states are located above and well separated from the unoccupied Fe 3d state configuration, which is located near the Fermi level. The 5d sub-band position in this reference is at 5 eV above the Fermi energy, which agrees with the observed O K- edge XMCD. This is the first time, where O K edge spectral XMCD features could be identified to antiferromagnetic coupling for different sub-lattices.

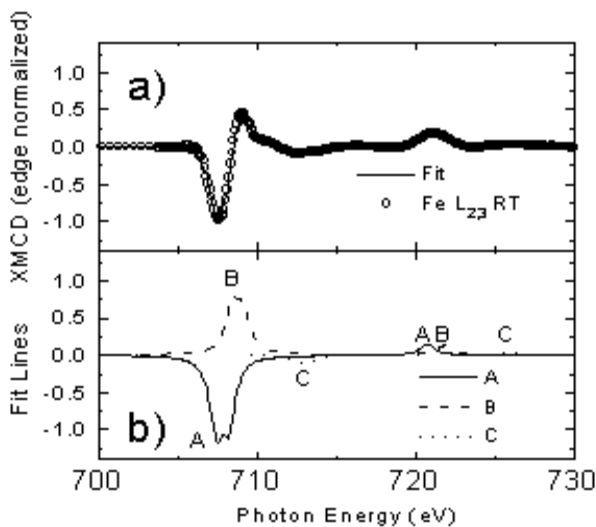


Figure 4: a) $\text{Fe L}_{2,3}$ XMCD at room temperature and corresponding fit result using momentum analysis. b) Three contributions (A, B and C) to the XMCD fit shown in a)

Comparing the shape of the $\text{Fe L}_{2,3}$ XMCD spectra in Fig. 1b with bulk Fe XMCD spectra (Chen 1995), an additional strong positive (negative for 80K) feature at 709 eV is observable. Two Fe^{3+} sub-lattices with different crystal symmetry and nearest neighbor coordination are present. Corresponding spectral features could be slightly separated in energy (Kawamura 1997). For a quantitative analysis we evaluated the Fe RT XMCD spectrum in terms of ground state moments (Thole 1993; van der Laan 1997; van der Laan 1998b). We used $\underline{w}^{000}(\propto n_h)$, $\underline{w}^{101}(\propto L_z)$ and $\underline{w}^{011}(\propto S_z)$ contributions. Details about this procedure has been published elsewhere (Goering 1999). The result of this fit and the corresponding XMCD spectrum from Fig. 1b are shown in Fig. 4a. The fit reproduces the spectrum nearly perfect. The major part of our spectrum could be represented by two prominent contributions which are indicated by A and B in Fig. 4b. A very small third

feature - which we will not further discuss here - is also present (Fig. 4b: C). The relevant parameters are: Fe L_3 - L_2 Spin Orbit coupling energy of 13.0eV, effective Fe 2p - 3d exchange constant of 0.8eV and a Lorentzian broadening of 0.95eV. The L_3 centers of energy are 707.8eV(A), 708.8eV(B) and 713.0eV(C). The values for the \underline{w}^{000} moments are 0.18(A) and -0.18(B). The \underline{w}^{000} moments reflect the number of 3d holes. Values for the $\underline{w}^{011}(S_z)$ moments are 3.16(A) and -1.32(B). The ratio is 2.39. According to the previous discussion this should be $3/2 = 1.5$ (Geller 1963; Neel 1964), denoting a slightly higher magnetic moment for the Fe^{3+} at tetrahedral sites (D) compared to octahedral sites (A) (Dunaevskii 1989). From the analysis of the $\underline{w}^{101}(L_z)$ moment we have 0.82(A) and -0.66(B). This indicates quite comparable orbital magnetic moments for the Fe^{3+} octahedral sites (D) and tetrahedral sites (A).

4. Conclusions

We have investigated the magnetism of HoIG quantitatively. Temperature dependant relative values are in quite good agreement with other data. Ho 4f magnetism is nicely represented by a $4f^0$ configuration, while the Fe magnetization is underestimated by a factor of two. We address this behavior to hybridization with oxygen ions. O K edge spectra show two different spectral features which could be identified to Fe 3d and Ho 5d contributions. Momentum analysis of Fe XMCD gives a separation between the two Fe sub-lattices and clearly reflects the ferrimagnetism present in the system.

5. Acknowledgments

This work was performed at BESSY I. We thank the BESSY beamline staff Heiko Gundlach for support and help. This work is financially supported by the BMBF (05SC8WW1) and DFG Forschergruppe Augsburg (Schu 964/2-3).

References

- Altarelli, M. (1993). Phys.Rev.B 47, 597 - 598
- Carra, P. et al. (1993). Phys.Rev.Lett. 70, 694 - 697
- Chen, C. T. et al. (1995). Phys.Rev.Lett. 75, 152 - 155
- Dartyge, E. et al. (1998). J.Alloys Comp. 275-277, 526 - 532
- Dunaevskii, S. M et al. (1989). Sov.Phys.Sol.State 31, 114 - 116
- Fischer, P. et al. (1992). Sol.State Com. 82, 857 - 861
- Geller, S. et al. (1965). Phys.Rev. 137, 1034
- Geller, S. et al. (1963). Phys.Rev. 131, 1080
- Goering, E. et al. (1999). J.Sync.Rad. 6, 537 - 539
- Goering, E. et al. (2000). J.Sync.Rad., submitted
- Hellwege, H. H. (1988). Einführung in die Festkörperphysik, Springer-Verlag, Heidelberg
- Kawamura, N. et al. (1997). Journal de Physique IV 7, 269 - 270
- Kittel, C. (1976). Introduction to Solid State Physics, Wiley & Sons, New York
- Knulle, M. et al. (1995). Sol.State Comm. 94, 267 - 273
- Maruyama, H. et al. (1995). Physica B 208-209, 760 - 762
- Neel, L. et al. (1964). Prog.low. temp.phys. 4, 344 - 383
- Pauthenet, R. (1958). J.Appl.Phys. 29, 253
- Pellegrin, E. et al. (2000). Journal de Physique IV 7, 405 - 408
- Rudolf, P. et al. (1991). J.Appl.Phys. 70, 6338 - 8979/91
- Rudolf, P. et al. (1992). J.MMM 109, 109 - 112
- Sette, F. et al. (1990). AIP Conf.Proc., 787 - 795
- Thole, B. T. et al. (1992). Phys.Rev.Lett. 68, 1943 - 1946
- Thole, B. T. and van der Laan, G. (1993). Phys.Rev.Lett. 70, 2499 - 2502
- van der Laan, G. et al. (1986). Phys.Rev.B 34, 6529 - 6531
- van der Laan, G. (1997). Phys.Rev.B 55, 8086 - 8089
- van der Laan, G. (1998a). Phys.Rev.B 57, 112 - 115
- van der Laan, G. (1998b). Phys.Rev.B 57, 5250 - 5258